

Article

On Melt Growth and Microstructure Characterization of Magnesium Bicrystals

Kevin Bissa ^{1,*}, Talal Al-Samman ¹  and Dmitri A. Molodov ^{1,2}

¹ Institute of Physical Metallurgy and Materials Physics, Rheinisch-Westfälische Technische Hochschule Aachen University, 52056 Aachen, Germany; tasamman@imm.rwth-aachen.de (T.A.-S.); molodov@imm.rwth-aachen.de (D.A.M.)

² International Research Organization for Advanced Science and Technology (IROAST), Kumamoto University, Kumamoto 860-8555, Japan

* Correspondence: bissa@imm.rwth-aachen.de

Abstract: Oriented magnesium bicrystals with a $45^\circ \langle 10\bar{1}0 \rangle$ asymmetrical tilt boundary were produced by directional solidification in a vertical Bridgman furnace. Employing a partition in the cylindrical mold led to unwanted crystallization on the contact surface with the growing interface, disrupting the desired growth conditions for the boundary. A modified setup with seed crystals placed side by side in a conical mold addressed the former issue and enabled the production of high-quality $56 \text{ mm} \times \varnothing 34 \text{ mm}$ bicrystals. Due to the asymmetrical character of the boundary, the adjacent growing crystals witnessed unequal growth rates, with the basal-oriented crystal dominating the growth process. Plane strain compression experiments were carried out on bicrystalline samples extracted from the prepared bicrystal. The panoramic orientation mapping of large areas of several mm^2 revealed low-angle boundaries (5° misorientation) associated with the curved segments of the original asymmetrical tilt boundary. It also depicted heterogeneous lattice rotation near the grain boundaries.

Keywords: magnesium; bicrystal; crystal growth; grain boundary panorama EBSD



Citation: Bissa, K.; Al-Samman, T.; Molodov, D.A. On Melt Growth and Microstructure Characterization of Magnesium Bicrystals. *Crystals* **2024**, *14*, 130. <https://doi.org/10.3390/cryst14020130>

Academic Editors: Yong Liu, Arnaud Magrez and David Wen Hua Bi

Received: 15 December 2023

Revised: 17 January 2024

Accepted: 21 January 2024

Published: 27 January 2024



Copyright: © 2024 by the authors. Licensee MDPI, Basel, Switzerland. This article is an open access article distributed under the terms and conditions of the Creative Commons Attribution (CC BY) license (<https://creativecommons.org/licenses/by/4.0/>).

1. Introduction

Over the last few decades, the specific mechanical properties of magnesium have prompted its substitution for conventional structural materials in various fields of application. Weight reduction is primarily decisive, such as in automotive, aerospace, and consumer electronics industries, and consequently, a comprehensive understanding of plastic magnesium's deformation behavior is crucial for optimizing manufacturing processes to ensure efficient and cost-effective production. In this context, the role of interfaces, in particular grain boundaries (GB), is of great importance due to their complex effects on grain boundary motion [1–4], stress concentration [5–9], texture evolution [10,11], recrystallization behavior [12], and electrical properties [13]. In order to continue with the development of advanced predictive crystal plasticity models that include GB effects, it is crucial to understand how the crystallography of the boundary and the orientations of the surrounding grains influence the plastic deformation response of the material. However, conducting such detailed investigations in polycrystals with curved grain boundaries poses significant challenges, since the structure (and consequently the inclination) changes continuously along a curved boundary [2]. It is therefore more suitable to carry out deformation experiments on specific grain boundaries with a well-known and constant crystallographic character. This can be achieved through the growth of bulk bicrystals with planar grain boundaries of a constant inclination and controlled misorientation. A common technique used for this purpose is diffusion bonding [14], where two single crystals with the desired orientations are joined together and annealed below the melting temperature. Over time, atomic diffusion across the interface of the two single crystals leads to the formation of a

solid bond, characterized by the presence of a clearly defined grain boundary between the two crystals. However, the presence of surface contaminants and defects during the joining process can result in the formation of pores or particles, ultimately impairing the quality and properties of the resulting boundary.

Another common technique is based on directional solidification in a vertical Bridgman furnace to produce specifically oriented bicrystals. During the slow cooling of the molten zone, the melt crystallizes on both seed crystals, leading to the growth of a cylindrical bicrystal with the desired misorientation. If the growth procedure is successful, the resulting boundary remains parallel to the growth direction. In the past, various bicrystals containing different types of grain boundaries out of copper [1,15,16], brass [17], nickel-base superalloy [18], and ferrosilicon alloy [19] were successfully grown using this method, which usually involves the seeded growth of single crystals with pre-selected orientations. Nowadays, the vertical Bridgman technique is widely used to grow semiconducting crystals due to the excellent electrical properties of single- and bicrystals [20–22]. In addition, the vertical Bridgman method was recently successfully used in deformation and microstructure studies on magnesium to investigate the mesoscopic interaction between dislocations and twin boundaries [8,23], as well as the accommodation of lattice rotations in the vicinity of the GB [10]. In most cases, a partition was used to separate the seeds to ensure a well-aligned grain boundary in the center of the cylindrical mold, but in contrast, Syed et al. [24] placed both seeds directly next to each other, which also resulted in a successful growing process. However, a critical analysis including an extensive understanding of the presented method, which could lead to an improvement of the crystal quality and the success rate, has not been carried out for magnesium, and is hence overdue.

The seeded growth technique can provide valuable macroscopic bicrystals that can be used to advance our understanding of the various properties of individual grain boundaries with regard to migration behavior, solute segregation, and plastic deformation. However, it can be quite challenging, primarily due to several complex factors and technical difficulties involved in the process. The aim of this paper is to provide further knowledge regarding the growth process of oriented Mg bicrystals by comparing two different mold setups using the vertical Bridgman technique, and to discuss their deformation behavior in plane strain compression at room temperature using panoramic optical and orientation microscopy. Therefore, the main research questions to be answered are: What difficulties (implied by the mold design) negatively affect the quality of the grown bicrystals, and can the commonly utilized mold design be optimized to increase the success rate?

2. Materials and Methods

The vertical Bridgman technique in this work was used with two different mold setups, as shown in Figure 1. The first setup A in Figure 1a features a conventional approach, where both semi-cylindrical seeds are positioned side by side, with a separating graphite partition located beneath the precursor material (polycrystalline blank). To ensure direct contact between the seeds and the blank, the mold is precisely positioned in the furnace, such that the blank material and the end of the seeds are melted in the hot zone. Lowering the mold away from the hot zone in the furnace moves the crystallization front upwards, maintaining uniform orientation in the upper volume. Both crystals grow simultaneously and separately until the crystallization front reaches the tip of the partition (Figure 1a). Continued crystallization in both crystals forms a flat boundary with the selected misorientation.

The second approach (mold setup B) is shown in Figure 1b. Both single-crystal seeds are positioned side by side, without the use of a partition, and centered beneath the blank. This configuration is similar to the growth procedure of a single crystal, except that it involves two semi-cylindrical seeds. Additionally, in contrast to mold setup A, the mold in this case is conical, with an opening angle of 4° . In this setup, the grain boundary is formed immediately upon traversing the molten zone and not at a distance from the starting position of the crystallization front.

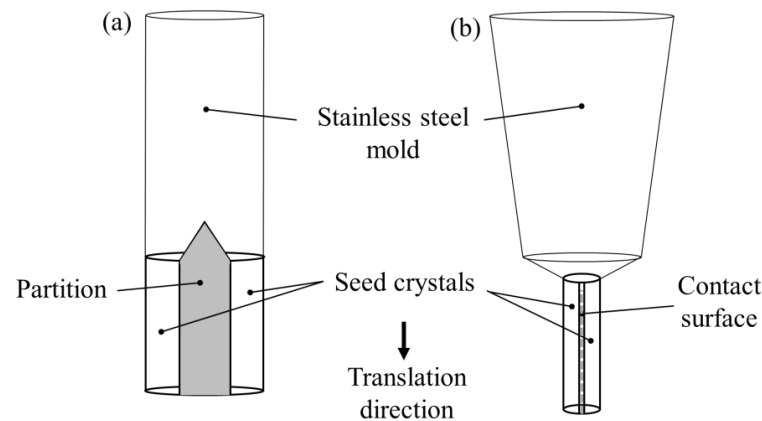


Figure 1. Schematic illustration of the mold setups A (a) and B (b) used in the current study to grow asymmetric Mg bicrystals.

In both setups, the stainless-steel molds were coated with graphite to prevent a reaction of the melt with the mold's inner surface. The cutting of the polycrystalline blank and the seed crystals was achieved by electric discharge machining (EDM). In this regard, magnesium single crystals were oriented at different angles to obtain distinct types of seeds, including those aligned parallel to the *c*-axis and those oriented at a 45° angle around the $\langle 10\bar{1}0 \rangle$ axis. The orientations of the seed crystals were examined using the X-ray Laue back-reflection method. The deviations from the desired orientations were less than 1°. The machined seed crystals and the polycrystalline blank were etched in a 5% nitric acid solution, followed by boiling in distilled water for several minutes to form an oxide layer on the surface. This layer served as a protective barrier to prevent diffusion-caused contamination during the growth process, and it facilitated the removal of the bicrystals from the mold. To ensure metallic contact between the two seed crystals and the blank, the oxide layers in the respective contact surfaces were removed through careful grinding with SiC paper.

An example of the used seeds and a polycrystalline blank is shown in Figure 2a. The mold in setup B containing the seeds and the blank was positioned in the hot zone of the induction coils in the furnace under a protective Argon atmosphere. This allowed for the seeds to partially melt and connect with the molten blank material (Figure 2b). After a holding time of 3 h at 720 °C, the mold was translated at a low velocity of 5 mm/h away from the induction coil to initiate the solidification process. At the beginning of the mold translation, the grain boundary was formed in the center of the seed compartment and traversed to the larger upper volume of the mold (Figure 2c). The whole procedure took approximately 21 h to complete, including 3 h for melting and homogenization and 18 h for the gradual solidification process. By that time, the entire material volume was extracted from the heating zone, and the grown bicrystal could be removed from the cooled mold. This was accomplished by turning the mold upside down and (in the case of slight adhesion) gently tapping it with a rubber hammer to loosen the bicrystal.

The top and bottom parts of the produced bicrystals were machined out by EDM, and the resulting surfaces were briefly ground and etched in HNO₃ to visualize the grain boundary and to ensure that the process was successful. The bicrystals were then sectioned into multiple slices of 6 mm thickness along the rod axis, and subsequently ground and etched to trace the position of the GB within each slice. For deformation experiments in a channel-die device, smaller samples measuring 14 mm in the longitudinal direction LD and 10 mm in the transverse direction TD were cut from each slice, such that the GB was consistently positioned at the center of each sample. To investigate the interaction of the grain boundary with the deformation mechanisms in the adjoining crystals, the bicrystalline specimens were compressed in the compression direction (CD) up to a maximum failure strain of 8%. The experimental details for the plane strain compression experiments are

given in [11]. Figure 3 shows the orientations of the (0002) and $\{11\bar{2}0\}$ poles of the bicrystal, along with the sample deformation geometry.

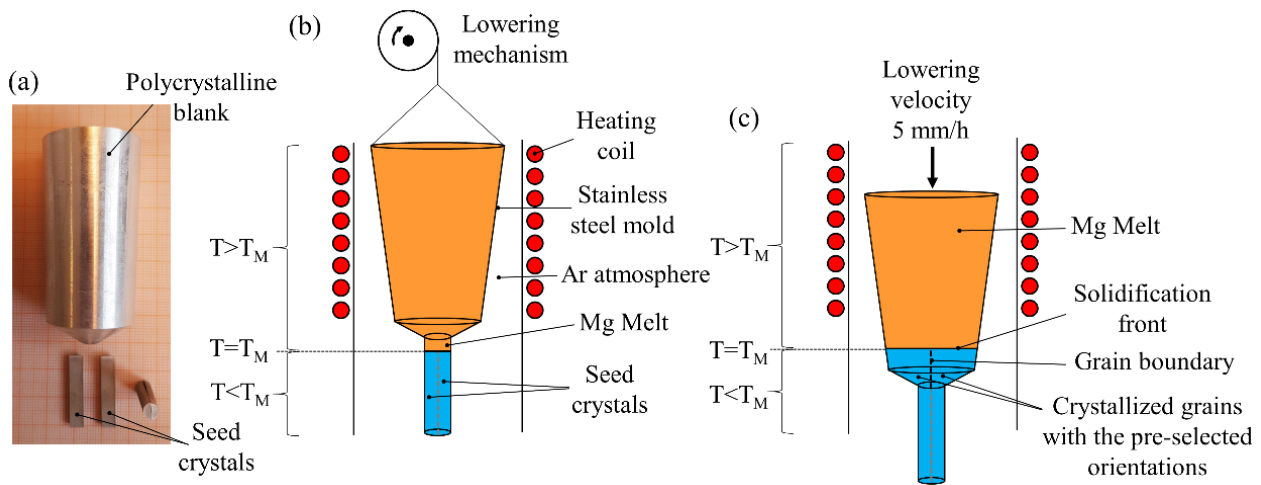


Figure 2. (a) Example of the polycrystalline blank and single-crystal seeds used for the growth experiments, (b) schematic illustration of mold setup B in the hot zone, and (c) the growth process of the bicrystal upon lowering the mold away from the induction zone.

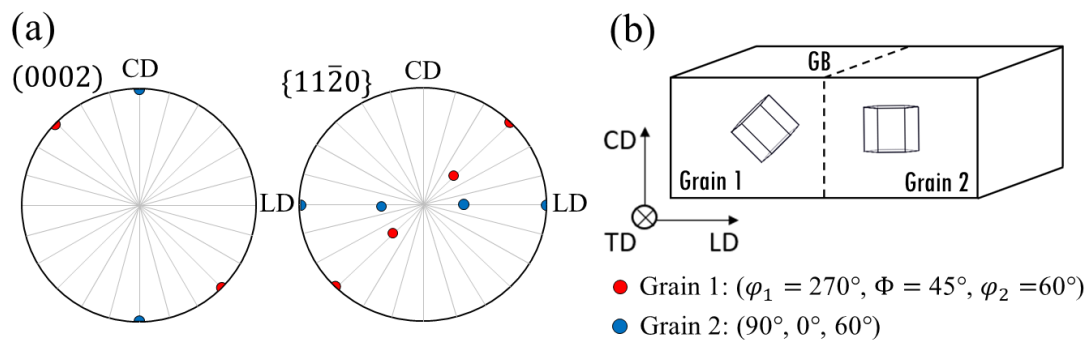


Figure 3. (a) Basal and prismatic pole figures depicting the initial grain orientations of the bicrystal used in the plane strain compression experiments at ambient temperature. (b) Schematic illustration of the specimen and the position of the $45^\circ \langle 10\bar{1}0 \rangle$ asymmetric tilt boundary, with respect to the deformation geometry.

After the deformation, the samples were cut in the middle of the $CD \times LD$ plane to avoid surface friction effects. The examined surface was subjected to metallographic preparation consisting of mechanical grinding and polishing with $3 \mu\text{m}$ and $1 \mu\text{m}$ diamond suspensions and electropolishing in a 5:3 ethanol/phosphoric acid electrolyte at 2 V. After the sample was removed from the electrolyte, a white phosphorus layer remained on the electropolished surface, necessitating a thorough rinse with running water. This led to the formation of a thin oxide layer on the surface, which was removed in the final preparation step through brief etching in 5% HNO_3 . Microstructure characterization was conducted using optical microscopy (Leica DMR, Wetzlar, Germany) and electron backscatter diffraction (EBSD) (Zeiss Leo Gemini 1530, Oberkochen, Germany). For optical microscopy, the surface was colored by brief etching in acetic acid picral solution, representing the local crystal orientation. To obtain a macroscopic view of the deformed microstructure, panoramic EBSD mapping was employed. This involved the measurement and stitching of approximately 1000 individual maps, each covering an area of $270 \times 190 \mu\text{m}$ with a step size of $4 \mu\text{m}$. The analysis of the EBSD data was performed using the MATLAB toolbox MTEX [25].

3. Results and Discussion

3.1. Mold Setup A

The removal of the grown bicrystals from the cylindrical mold in setup A was problematic due to the strong adhesion of the crystals to the mold, despite the applied graphite coating. This required applying force to the bottom part of the mold for extraction, which led to macroscopic deformation of the grown bicrystal, thereby rendering it unsuitable for further experiments. Moreover, the formation of small, undesired crystals on the surface of the partition (as seen in Figure 4) had a detrimental impact on the quality of the experiment. Hence, to overcome this limitation, the new, improved setup B was developed and used instead to avoid the nucleation of defects at the growing interface.

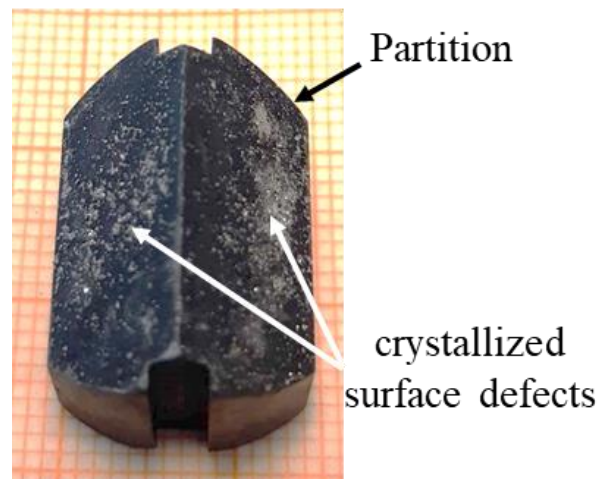


Figure 4. Contact surface of the partition after a crystal growth experiment, showing unwanted surface defects.

3.2. Mold Setup B

Compared to the previous setup, the as-grown bicrystals grown using setup B were much easier to extract from the mold. This was due to the conical mold design and the associated reduction in adhesion effects. With this setup, it was also possible to grow symmetrical tilt grain boundaries, as demonstrated in [11]. During the experiments, the grain boundary grew out of the desired position in the center of the mold and came out of the grown bicrystal as a curved boundary (Figure 5). This behavior indicates that the growth rate of both seed crystals differs due to different crystallographic solid/melt interfaces and growth directions. In the literature, this is referred to as a non-isoaxial growth condition [26–28], where an unequal undercooling is required for the growth of both crystals. In the present case, this implies that grain 2 with its [0001] axis aligned with the growth direction grows into grain 1, subsequently causing the grain boundary to deflect in that direction. As a result, the basal-oriented grain 2 dominated the growth process. In a related context, it is anticipated that the growth of a twist grain boundary would encounter a similar problem, resulting in a rotation of the grain boundary around the growing direction, which was observable in several attempts as well. The growth rate variation in the two growing crystals acted parallel to the grain boundary, leading to different growth rates in the rear and front volumes of each grain. The utilization of mold setup B significantly decreased the number of growing processes due to the improved quality of the bicrystals. Due to the absence of the partition as it was used in [1,15–17], grain boundary formation started in the volume of the molten seeds. As a consequence, the grain boundary sometimes grew in a curved shape or grew immediately towards the cylindrical mold wall next to the seed, not even reaching the larger conical volume at the top. A commonly utilized partition of the seeds can prevent such behavior, but at the same time, it can also generate other problems, as described in Section 3.1.

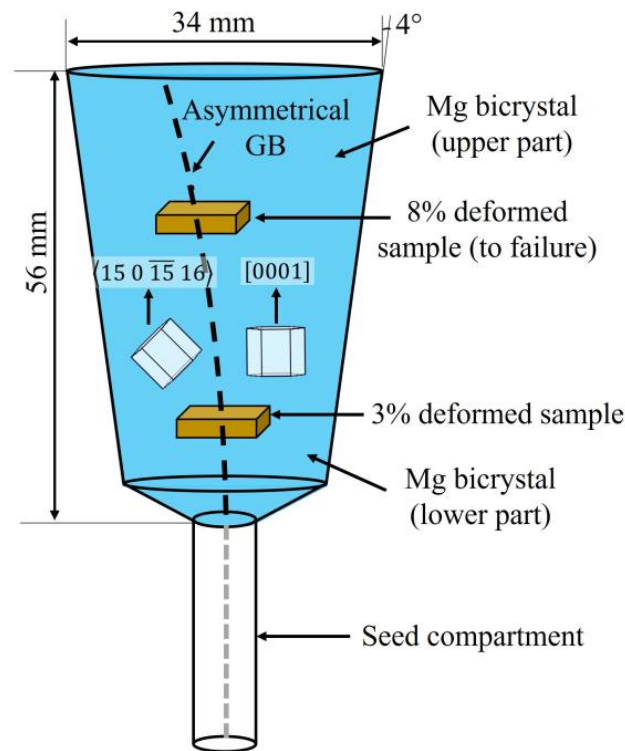


Figure 5. Resulting shape of the $45^\circ \langle 10\bar{1}0 \rangle$ asymmetric tilt boundary due to different growth rates of the two crystals. The schematic also shows the location of the extracted compression samples from the as-grown bicrystal.

3.3. Microstructure Characterization

Figure 6 shows the results of the microstructure characterization of the 3% deformed sample, which was carried out using panoramic optical and orientation microscopy (EBSD). The optical image presented in Figure 6a depicts a mostly flat GB in the bottom section of the sample, extending approximately 3 mm along the sample direction CD. However, in the upper region of the sample, the optical image shows a protrusion in the GB structure within grain 2. To investigate the nature of this feature, the outlined region in Figure 6a (yellow rectangle) was measured by large-area EBSD mapping to obtain orientation and misorientation data of the boundary and bulk regions. The inverse pole figure (IPF) map in Figure 6b reveals that the protrusion of the $45^\circ \langle 10\bar{1}0 \rangle$ boundary is associated with the presence of two low-angle grain boundaries that run almost parallel to CD. Interestingly, this observation was only made in the 3% deformed sample, and not in the higher deformed sample extracted from the upper volume of the bicrystal (Figure 5). The asymmetrical misorientation of the grain boundary and the longer duration of the lower volume in the furnace suggest a potential involvement of thermally driven boundary migration [4,29,30]. This phenomenon might have contributed to the macroscopic convexity of the grain boundary within grain 2. Consequently, what remains is a low-angle grain boundary occupying the initial position of the grain boundary. In the upper volume of the bicrystal, this process was prevented by the removal of the mold from the furnace, which took place once the bicrystal had fully solidified.

In Figure 6c, the orientations of grain 1 and grain 2, including that of the sub-grain in grain 2, are displayed in the basal and prismatic pole figures. To evaluate the misorientation at the grain boundaries after the small deformation, an orientation profile along the line scan A-B-C-D-E, parallel to LD, is plotted in Figure 6d. The orientation data starting from point A show some fluctuations in the bulk of grain 1 that might be due to some heterogeneous lattice rotation in that region by favored basal slip. The crystal orientation near the GB region remains closely aligned with the initial orientation of $\Phi = -45^\circ$ relative to grain 2 ($\Phi = 0^\circ$). At point B, the misorientation profile exhibits a sudden change in

misorientation angle of $\Delta\Phi = 43^\circ$, signifying an orientation transition from grain 1 to grain 2. At points C and D, the measured drops in orientation are about 5° , which corresponds to both low-angle grain boundaries in grain 2. The plateau extending up to point E marks the ideal basal orientation in grain 2, where basal slip is geometrically hard to activate due to a Schmid factor of zero.

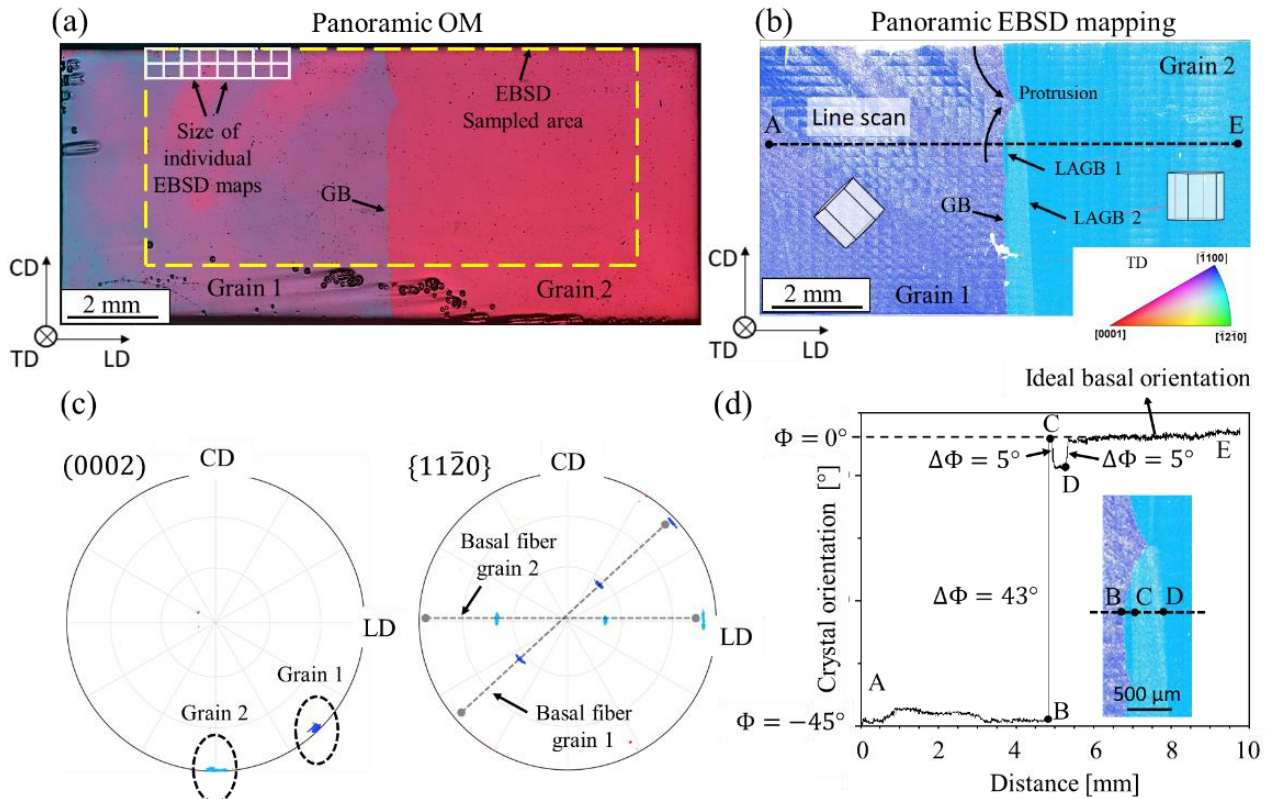


Figure 6. Microstructure characterization of the 3% deformed bicrystalline sample. (a) Panoramic optical image of the CD-LD mid-plane, (b) panoramic IPF orientation map (color-coding with respect to sample direction TD), (c) corresponding basal and prismatic pole figures, and (d) orientation profile along the marked line scan in (b). $\Delta\Phi$ in the plot represents sudden changes in orientation associated with grain boundaries.

Figure 7 shows the results of the sample deformed to failure at a strain of 8.3%. The panoramic optical micrograph (Figure 7a) depicts a planar grain boundary that is slightly inclined at an angle of 8° from the compression axis. The figure also illustrates macroscopic cracks at 45° from the compression axis, which are a result of shear failure, given the hard orientation of grain 2. The IPF map in Figure 7b shows no indications of low angle boundaries near the main asymmetric boundary. Grain 1 contained a bundle of deformation twins that are most likely of the $\{10\bar{1}2\}$ tension type, judging by the position of their (0002) poles relative to the position of the parent matrix in grain 1 (Figure 7c). To evaluate the lattice rotation in grain 1, which was initially favorably oriented for basal slip, an additional map was introduced in Figure 7d. The color-coding in this map represents the angular deviation from the initial orientation, characterized by a lattice rotation about the TD axis. For example, $\Phi < 5^\circ$ corresponds to a slight lattice rotation, which obviously applies to grain 2 (blue color) since simple shear by basal slip was highly restricted during deformation. Deformation mechanisms that can accommodate strain along the c-axis require thermal activation. Hence, at room temperature, shear localization culminating in macroscopic failure was to be expected. An interesting feature in Figure 7d is seen in grain 1, exhibiting a non-uniform orientation spread in the CD-LD plane. The rotation of the initial lattice

seems to be localized within a deformation band of higher Φ values, ranging between 15° and 20° . For more insights into this phenomenon, the reader is referred to [11].

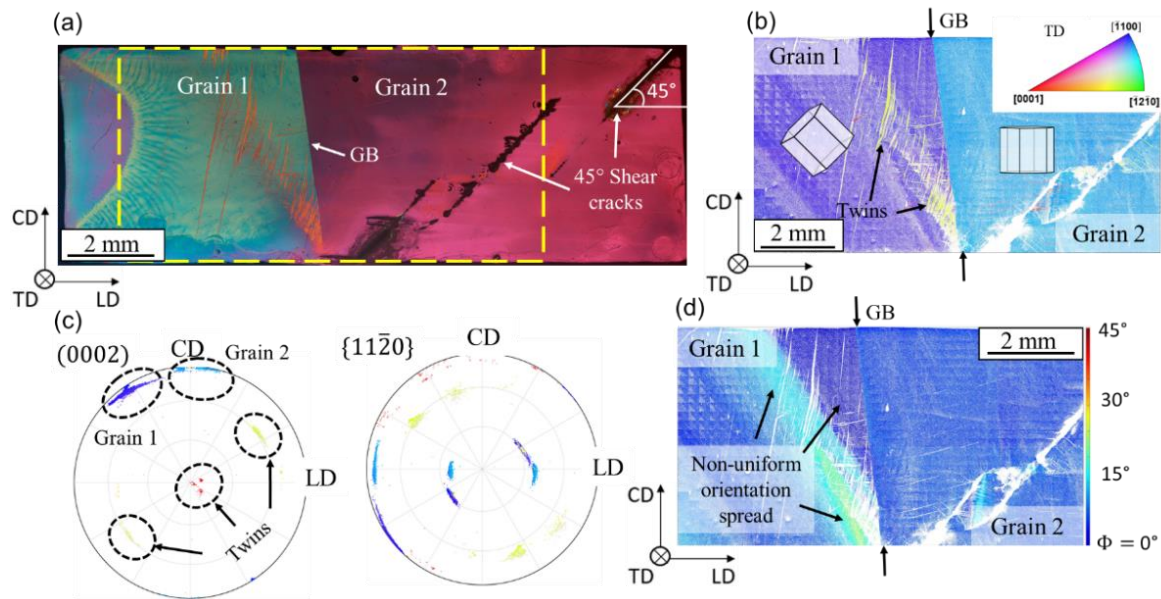


Figure 7. Microstructure characterization of the 8.3% deformed bicrystalline sample to failure. (a) Panoramic optical image of the CD-LD mid-plane, (b) panoramic IPF orientation map (color-coding with respect to sample direction TD), and (c) corresponding basal and prismatic pole figures. (d) Orientation spread map, with Φ indicating the angular deviation from the initial grain orientation. The map reveals the lattice rotation around TD caused by dislocation slip.

4. Conclusions

1. The conventional mold setup using a partition to separate the seed crystals in a cylindrical mold led to certain experimental limitations characterized by the formation of small crystals at the contact surface with the melt near the growing interface. This undesired effect impaired the optimal growth condition of the targeted boundary by introducing unwanted grains to the grain boundary region.
2. An improved setup was designed wherein the seed crystals were placed side by side within a conical-shaped mold. This design not only allowed the production of high-quality bicrystals featuring well-defined flat boundaries, but it also simplified the delicate process of extracting the bicrystal from the mold after cooling and significantly increased the success rate of producing high-quality bicrystals.
3. Different crystallographic growth axes in the adjacent crystals led to different growth rates. This broke the growth symmetry of the bicrystal, causing a deflection of the grown boundary from its original position in the center of the mold. The growth process was thus dominated by the basal-oriented crystal with its crystallographic c-axis parallel to the growth direction.
4. In the samples extracted from the lower portion of the bicrystal, orientation imaging microscopy revealed low angle boundaries (5° misorientation) associated with curved segments of the initial bicrystal boundary. This behavior is likely linked to the asymmetrical configuration of the bicrystal and the longer annealing duration of its lower part during the slow solidification process. By comparison, the deformation sample extracted from the upper part of the bicrystal (much shorter annealing duration) depicted no signs of thermally driven boundary migration. The boundary was flat and slightly inclined with respect to the loading axis. Shortening the duration during which the lower part is influenced by heat conduction from the hot zone would enhance the quality of the resulting boundary. However, it would also lead to the production of smaller bicrystals.

5. The use of panoramic orientation mapping to investigate the deformation behavior of the bicrystal demands considerable resources and time. Nevertheless, it offers valuable access to orientation and misorientation data on a macroscopic scale. This is crucial, considering the heterogeneity of strain distribution and lattice rotation in the vicinity of the grain boundary region.

Author Contributions: Conceptualization, K.B., T.A.-S. and D.A.M.; methodology, K.B.; software, K.B.; validation, K.B., T.A.-S. and D.A.M.; investigation, K.B.; resources, K.B.; data curation, K.B.; writing—original draft preparation, K.B.; writing—review and editing, T.A.-S. and D.A.M.; visualization, K.B. and T.A.-S.; supervision, K.B.; project administration, T.A.-S. and D.A.M.; funding acquisition, T.A.-S. and D.A.M. All authors have read and agreed to the published version of the manuscript.

Funding: The authors express their gratitude to the Deutsche Forschungsgemeinschaft (DFG) for financial support (MO 848/18-2).

Data Availability Statement: The original contributions presented in the study are included in the article, further inquiries can be directed to the corresponding author/s.

Acknowledgments: They also thank Arndt Ziemons (IMM, RWTH Aachen) for his valuable assistance with the crystal growth experiments.

Conflicts of Interest: The authors declare no conflicts of interest.

References

1. Chen, F.; Dixit, G.; Aldykiewicz, A.J.; King, A.H. Bicrystal studies of diffusion-induced grain boundary migration in Cu/Zn. *Metall. Trans. A* **1990**, *21*, 2363–2367. [\[CrossRef\]](#)
2. Winning, M.; Gottstein, G.; Shvindlerman, L.S. Stress induced grain boundary motion. *Acta Mater.* **2001**, *49*, 211–219. [\[CrossRef\]](#)
3. Liu, X.; Wang, J. Low-energy, Mobile Grain Boundaries in Magnesium. *Sci. Rep.* **2016**, *6*, 21393. [\[CrossRef\]](#) [\[PubMed\]](#)
4. Homer, E.R.; Holm, E.A.; Foiles, S.M.; Olmsted, D.L. Trends in Grain Boundary Mobility: Survey of Motion Mechanisms. *JOM* **2014**, *66*, 114–120. [\[CrossRef\]](#)
5. Sun, S.; Adams, B.L.; King, W.E. Observations of lattice curvature near the interface of a deformed aluminium bicrystal. *Philos. Mag. A* **2000**, *80*, 9–25. [\[CrossRef\]](#)
6. Zaeferrer, S.; Kuo, J.-C.; Zhao, Z.; Winning, M.; Raabe, D. On the influence of the grain boundary misorientation on the plastic deformation of aluminum bicrystals. *Acta Mater.* **2003**, *51*, 4719–4735. [\[CrossRef\]](#)
7. Tokuda, Y.; Tsurekawa, S.; Molodov, D.A. Local mechanical properties in the vicinity $(1\bar{1}0)\Sigma 3/[111]$ symmetric tilt grain boundary in aluminum bicrystal. *Mater. Sci. Eng. A* **2018**, *716*, 37–41. [\[CrossRef\]](#)
8. Brandenburg, J.-E.; Seo, J.; Molodov, D.A.; Tsurekawa, S. Influence of symmetrical $\langle 10\bar{1}0 \rangle$ high-angle tilt grain boundaries on the local mechanical properties of magnesium bicrystals. *Mater. Sci. Eng. A* **2021**, *826*, 141913. [\[CrossRef\]](#)
9. Barrales-Mora, L.A.; Tokuda, Y.; Molodov, D.A.; Tsurekawa, S. On incipient plasticity in the vicinity of grain boundaries in aluminum bicrystals: Experimental and simulation nanoindentation study. *Mater. Sci. Eng. A* **2021**, *828*, 142100. [\[CrossRef\]](#)
10. Schreiber, M.; Molodov, K.D.; Al-Samman, T.; Molodov, D.A. On the role and alteration of grain boundaries in/during accommodating plasticity in magnesium. *Acta Mater.* **2020**, *191*, 124–130. [\[CrossRef\]](#)
11. Bissa, K.; Al-Samman, T.; Molodov, D.A. Deformation behaviour of magnesium bicrystals with symmetrical $90^\circ \langle 11\bar{2}0 \rangle$ tilt grain boundaries analysed by large area EBSD mapping. *J. Magnes. Alloys* **2023**, *11*, 1556–1566. [\[CrossRef\]](#)
12. Guan, D.; Rainforth, W.M.; Ma, L.; Wynne, B.; Gao, J. Twin recrystallization mechanisms and exceptional contribution to texture evolution during annealing in a magnesium alloy. *Acta Mater.* **2017**, *126*, 132–144. [\[CrossRef\]](#)
13. Li, X.; Zhu, Z.; Behnia, K. A Monomaterial Nernst Thermopile with Hermaphroditic Legs. *Adv. Mater.* **2021**, *33*, e2100751. [\[CrossRef\]](#) [\[PubMed\]](#)
14. Muschik, T.; Hofmann, S.; Gust, W. A novel technique to study grain boundary and surface segregations under identical conditions with AES. *Scr. Metall.* **1988**, *22*, 349–354. [\[CrossRef\]](#)
15. Russell, J.D.; Winter, A.T. Orientation effects in embrittlement of copper bicrystals by bismuth. *Scr. Metall.* **1985**, *19*, 575–579. [\[CrossRef\]](#)
16. Schwarz, S.M.; Houge, E.C.; Giannuzzi, L.A.; King, A.H. Bicrystal growth and characterization of copper twist grain boundaries. *J. Cryst. Growth* **2001**, *222*, 392–398. [\[CrossRef\]](#)
17. Zeng, Z.; Rek, Z.; Bilello, J.C. In-situ quasi-real time observations of the deformation of α -brass bicrystals via synchrotron x-ray topography. *MRS Online Proc. Libr.* **1993**, *307*, 225. [\[CrossRef\]](#)
18. Chen, G.S.; Aimone, P.R.; Gao, M.; Miller, C.D.; Wei, R.P. Growth of nickel-base superalloy bicrystals by the seeding technique with a modified Bridgman method. *J. Cryst. Growth* **1997**, *179*, 635–646. [\[CrossRef\]](#)
19. Lejček, P.; Bartuška, P.; Lašek, J. Growth of alloy bicrystals with twist grain boundaries by the floating zone technique. *J. Cryst. Growth* **2005**, *275*, e1597–e1602. [\[CrossRef\]](#)

20. Jin, M.; Yang, W.-H.; Wang, X.-H.; Li, R.-B.; Xu, Y.-D.; Xu, J.-Y. Growth and characterization of ZnTe single crystal via a novel Te flux vertical Bridgman method. *Rare Met.* **2021**, *40*, 858–864. [[CrossRef](#)]
21. Wasim, S.M.; Rincón, C.; Marín, G.; Delgado, J.M.; Contreras, J. Effect of ordered defects on the crystal structure of In-rich ternary compounds of the Cu–In–Se system. *J. Phys. D Appl. Phys.* **2004**, *37*, 479–484. [[CrossRef](#)]
22. Dong, J.; Jie, W.; Yu, J.; Guo, R.; Teichert, C.; Gradwohl, K.P.; Zhang, B.B.; Luo, X.; Xi, S.; Xu, Y. Twin boundary dominated electric field distribution in CdZnTe detectors. *Chin. Phys. B* **2018**, *27*, 117202. [[CrossRef](#)]
23. Molodov, K.D.; Al-Samman, T.; Molodov, D.A. Profuse slip transmission across twin boundaries in magnesium. *Acta Mater.* **2017**, *124*, 397–409. [[CrossRef](#)]
24. Syed, B.; Catoor, D.; Mishra, R.; Kumar, K.S. Coupled motion of [10–10] tilt boundaries in magnesium bicrystals. *Philos. Mag.* **2012**, *92*, 1499–1522. [[CrossRef](#)]
25. Bachmann, F.; Hielscher, R.; Schaeben, H. Texture Analysis with MTEX—Free and Open Source Software Toolbox. *SSP* **2010**, *160*, 63–68. [[CrossRef](#)]
26. Chalmers, B. Melting and Freezing. *J. Miner. Met. Mater. Soc.* **1954**, *6*, 519–532. [[CrossRef](#)]
27. Anderson, P.A. The Molecular Process of Crystal Growth in Hexagonal Metals. Deposition upon Monocrystalline Hemispheres of Zinc. *Phys. Rev.* **1932**, *40*, 596–606. [[CrossRef](#)]
28. Adámek, J.; Lejček, P. Melt growth of non-isoaxial bicrystals of an Fe–3%Si alloy. *J. Cryst. Growth* **2000**, *211*, 461–465. [[CrossRef](#)]
29. Mullins, W.W. The effect of thermal grooving on grain boundary motion. *Acta Metall.* **1958**, *6*, 414–427. [[CrossRef](#)]
30. Gottstein, G.; Shvindlerman, L.S. *Grain Boundary Migration in Metals*; CRC Press: Boca Raton, FL, USA, 2009.

Disclaimer/Publisher’s Note: The statements, opinions and data contained in all publications are solely those of the individual author(s) and contributor(s) and not of MDPI and/or the editor(s). MDPI and/or the editor(s) disclaim responsibility for any injury to people or property resulting from any ideas, methods, instructions or products referred to in the content.